Single Packet, Single Channel, Switched Antenna Array for RF Localization

YANG-HSI SU, University of Michigan, USA
CHOUCHANG (JACK) YANG, University of Michigan, USA
EUISEOK HWANG, Gwangju Institute of Science and Technology, Korea
ALANSON P. SAMPLE, University of Michigan, USA

Fig. 1. This work uses an 8-element switched antenna array with a single chain receiver shown in (a) to estimate the AoA of commodity BLE devices. A phone transmitting BLE packets is carried in the user's pocket shown in (b), while the user walks around the space. A technical evaluation in a low-multipath lobby environment (c) and a real-world usage evaluation with multiple users are conducted. The 2D trace of the user shown in (e) combines the AoA estimations from two antenna arrays.

Cost-effective and accurate means of localizing radio transmitters has the potential to enable a wide range of applications in the consumer electronics, IoT, and healthcare domains. However, existing multi-antenna localization methods require high-cost synchronized receivers, long integration times, and/or specialized packet structures. This paper proposes using a high-speed RF mux that sequentially connects antennas to a single 2MHz radio receiver and sub-packet switching to determine the Angle of Arrival of individual packets. Importantly, this approach does not need synchronization between the mux and the receiver, reducing cost and system complexity. Our signal processing pipeline recovers both switch timing and the antenna number from the received RF signal. The sub-packet waveforms are used to generate a synthetic reference packet, and our customized Multi-Resolution Beaming and MUSIC algorithms are used to determine the Angle of Arrival. Results show that our real-time system is highly accurate even when the target is moving, with a mean AoA accuracy of 3.4 degrees and a 2D localization accuracy of 36.4 cm. Furthermore, the system is capable of tracking multiple users carrying smartphones in either their hands or pockets. Ultimately this approach enables a single low-cost, low bandwidth commodity RF receiver to be used to create an N-element phased array receiver.

CCS Concepts: • **Networks** → **Location based services**; • **Human-centered computing** → *Ubiquitous and mobile computing*.

Additional Key Words and Phrases: Localization, Single Packet, Single Receiver, AoA

Authors' addresses: Yang-Hsi Su, University of Michigan, Ann Arbor, MI, USA, devilsu@umich.edu; Chouchang (Jack) Yang, University of Michigan, Ann Arbor, MI, USA, ccjack182@gmail.com; Euiseok Hwang, Gwangju Institute of Science and Technology, Korea, euiseokh@gist.ac.kr; Alanson P. Sample, University of Michigan, Ann Arbor, MI, USA, apsample@umich.edu.

1 INTRODUCTION

Effective means of determining the location of users, computing devices, and tag objects remain a key enabling technology of many innovative applications such as indoor navigation [13, 17], healthcare and assisted living [6, 10, 36], smart homes [3, 19], augmented reality [16, 24, 35], as well as the Internet of Things (IoT) [11, 26, 40]. Both academic and industry researchers have investigated a wide variety of radio-based localization approaches, algorithms, and deployment strategies [44, 49]. All of which have attempted to balance hardware cost and complexity, compatibility with existing devices, and localization accuracy.

To meet this need many research efforts have focused on re-purposing existing wireless access points and gateways as localization anchors in order to reduce deployment costs. These software-based approaches use channel information such as Received Signal Strength Indicator (RSSI) measured from a single antenna (or multiple independent antennas) and employ advanced signal processing, fingerprinting, and machine learning techniques to localize mobile transmitters. While these software-only approaches excel in terms of hardware simplicity and deployability, due to channel fading and multi-path propagation, localization accuracy is generally between 2m-5m [7, 49], limiting their utility for many applications.

In contrast, antenna designers have long explored the use of large element phased antenna arrays, which have been shown to have excellent localization accuracies as low as 23cm [46] and Angle of Arrival (AoA) estimation error as low as 1.5° to 0.4° [4, 25]. The key insight is that multiple antennas provide both path diversity and the ability to measure the phase difference of the RF wavefront in order to determine the direction of the mobile device. However, these approaches require synchronized receivers for each antenna element in the array and/or complicated beam steering mechanisms, which significantly increases cost and system complexity. Furthermore, the lack of cost-effective radio hardware capable of receiving more than three channels hinders research efforts and ultimately limits the deployability of many innovative localization solutions and applications.

This creates a challenge: *"How can we use low-cost, single-channel RF radio chip sets to create large element antenna arrays without requiring complex and costly synchronization hardware?"* In order to meet this challenge, this work proposes a fully **asynchronous** methodology for creating large switched antenna, single receiver arrays, capable of localizing mobile RF transmitters in real-time. This signal processing only approach does not require a second RF receiver channel to recover the switch timing or a complex hardware-specific method to synchronize the receiver and RF switch. Instead, timing information and antenna ID are recovered from the discontinuities induced on the received waveform caused when the RF MUX switches between antennas. This creates its own set of challenges since 1) the discontinuities disrupt the data modulated on the packet and 2) the discontinuities are only present when actively receiving radio traffic, meaning the antenna number and timing can not be tracked between packets. To overcome these challenges, we introduce a sub-packet switching approach that enables each antenna in the array to sample an individual packet one or more times, providing sufficient switch discontinuity events to recover the switch state, enough data to compute the Carrier Frequency Offset (CFO), and ultimately data to compute the Angle of Arrival (AoA) of individual packets. This, combined with our new phase derivative-based packet detection and symbol decoding approach, allows the system to robustly identify hidden discontinuity events buried in the data and decode packets robustly compared to magnitude-based decoding schemes.

To demonstrate the validity of this approach, a custom-designed 8-element patch antenna array has been constructed using an 8:1 RF Switch connected to a single port of a Software Defined Radio (SDR) and Bluetooth 4.0 has been selected as a target protocol for mobile device localization. Results show that the system can effectively

detect and decode a packet received by the time-multiplexed antenna array. In order to perform Angle of Arrival estimation, a synthetic reference packet is generated and used to calculate the phase difference of arrival for each of the switched antenna waveform samples. This phase information is then processed by our customized Multi-Resolution Beaming and MUSIC (MUltiple SIgnal Classification) algorithms that were modified to work with asynchronous switched antenna arrays. Results show that the system is highly accurate with a single packet AoA accuracy of 5.14°and a five packet median filtered one of 3.44°, which can enable tracking of fast objects or hard to detect transmitters. Additionally, using two AoA receivers, our real-time system is capable of localizing mobile users in 2D carrying commodity IOS and Android smartphones, with a line-of-sight average 2D localization error of 36.4 cm and 40.4 cm average error when the phones are hidden in their pockets. Ultimately this approach is generalizable to a wide variety of protocols and encoding schemes using single-carrier frequency such as UHF RFID, Zigbee, Sigfox, and Z-wave. Thus enables a low-cost, low bandwidth single channel receiver to be used to create an 'N' element phased array.

This paper makes the following contributions:
- An asynchronous switch and receiver approach for switched antenna arrays
- A phase derivative packet detection and symbol decoding approach
- A sub-packet sampling approach that enables single packet AoA
- A synthetic reference packet for phase difference of arrival calculation
- Extracting full antenna correlation matrix from sparse switched antenna data for MUSIC
- Robust, real-time AoA and 2D localization of commodity smartphones

2 RELATED WORKS

Radio Frequency (RF) based indoor localization systems have received a significant amount of attention as researchers have sought to create location-aware services and applications. These systems often take advantage of existing wireless infrastructure and products to reduce deployment challenges and leverage the unique physical layer features of their respective protocols to improve localization performance. Examples include long-distance localization FM (frequency modulation) [12] and WiFi [30, 46], ZigBee, [9], RF Identification (RFID) [5, 39], Ultra Wide Band (UWB) [50], and Bluetooth [18] for mid to short localization distances. In particular, this work focuses on Bluetooth not only because it is widely used, with an estimated 4.7 billion devices sold in 2022, but also since the underlining physical Gaussian Frequency-Shift Keying (GFSK) modulation scheme is similar to other IEEE 802.15.4 systems operating in the 2.4 GHz frequency band. Allowing a pathway for our single packet, switched antenna Array localization approach to be applied to wireless protocols such as UHF RFID, Zigbee, Sigfox, Z-wave, BLE, etc.

2.1 Radio Hardware and Software Defined Radios

One of the most challenging aspects of creating antenna arrays with a large number of elements is the need for low-cost and easy-to-use multi-channel receiver chipsets and hardware platforms. Especially considering that, in order to measure the minute phase differences of the incoming RF wave as captured by each antenna, each RF receiver chain must be precisely synchronized with each other.

Examples include the Analog Devices AD9361, which is a coherent, fully duplexed, 2x transmitter and 2x receiver IC that has enabled many innovative, Multiple-Input and Multiple-Output (MIMO) capable hardware platforms such as the Ettus Research B210 Universal Software Radio Peripheral (USRP). However, the complexity of adding additional transmitter/receiver signal chains on chip increases substantially with additional channels, and as a result, few ICs with more than two channels are available due to market forces. Notable exceptions include the Intel 5300 NIC [23] and the Atheros NIC cards [45], each with 3 transceiver chains that are capable of reporting channel state information (CSI). The alternative is to synchronize individual receiver chips at the board

level or module level by driving each with a common reference clock. While this approach can be effective, it also significantly increases complexity and system cost which does not make it practical for commercially viable and widely deployable applications.

Towards this goal, many research efforts have sought to reduce the number of RF receiver chains by using high-speed RF switches to sequentially connect multiple antennas to the input of one or more receivers. Notable examples include Xie et al. [48], which uses 4:1 RF switches attached to each of the three input ports of an Atheros NIC card to create a 12-element switched antenna. In this approach, the three RF channels are inherently synchronized by the Qualcomm AR9580/90 chipset, and the timing synchronization of the three 4:1 switches is done via ethernet over custom modified Linux TCP sockets. A more direct approach was demonstrated in Gjengset et al. [21], where a five-element array was created using two Intel 5300 NICs. Here one of the antennas is connected to an RF splitter which sends identical signals to both cards for synchronization. In Adib et al. [2] created a 20-element antenna array using 4:1 RFs switches and multiple N210 USRPs synchronized by an external clock. In order to recover the timing of the switches, an additional synchronized N210 USRP was used to capture control pulses sent via an Arduino through the RF signal path. Finally, Gu et al. [22] used a single RF receiver and 8:1 RF switches, thus reducing the need for a channel to channel synchronization. However, in order to recover the antenna switch state, low-level control over the SDR's internal FPGA was required to inject the antenna ID into the metadata for each RF sample, thus requiring tight timing control and strict synchronization between the RF switch and receiver. Furthermore this approach requires a minimum of 21 consecutive packets in order to make a single Angle of Arrival estimation resulting in higher latency and loss of tracking due to packet collisions.

In contrast our approach only requires a single radio receiver with 2MHz of bandwidth (standard for BLE receivers) and does not require and synchronization or electrical connection to the RF switch. As a result our approach allows viable path forward to integrate AoA and locationing capabilities into a wide number of chips sets and radio modules. Furthermore, our single packet approach allows for fast target acquisition and tracking of commercially available smartphones and IoT devices that transmit at 30 packets per second or less.

2.2 Localization Approaches

One of the most commonly used low-level RF channel parameters to locate a target device is RSSI. This approach has been explored in various technologies, such as LoRa [28], WiFi [13], and BLE [11, 29, 32, 33]. RSSI-based

Table 1. A summation of RF localization systems

Manuscript	Radio Technology	Approach	Tx	Rx	RF Environment	Room Size	Multi-User	AoA Accuracy		Localization Accuracy	
								Mean	Median	Mean	Median
Chintalapudi et al [13]	WiFi	RSSI \ Fingerprinting	Existing WiFi APs	phone	Office \ Constrained	140m x 90m	Single User			~2 m	
Lin et al [29]	BLE	RSSI \ Fingerprinting	BLE beacons	phone	Indoor \ Constrained	40m x 16m	Multi-User			3~5 m	
Phutcharoen et al [33]	BLE	RSSI \ Fingerprinting	BLE beacons	phone	Office \ Constrained	9m x 10.2m	Single User			1.3 m	
Peng et al [32]	BLE	RSSI \ Fingerprinting	unknown	Office \ Unconstrained	16.8m x 12.6m	Single User			~3 m	
Chen et al [11]	BLE	RSSI+MAG+IMU \ Sensor Fusion	BLE beacons	phone	Office, Home, Outdoor \ Unconstrained	9m x 11m 16m x 15m	Single User			1.8m (indoor) 1.2m (outdoor)	
Choi et al [14]	WiFi	RSSI+TOA \ Deep Learning	WiFi APs	Phone	Office \ Unconstrained	56m x 37m	Multi-User				~1.8 m
Wang et al [42]	WiFi	CSI \ Deep Learning	WiFi APs	IWL 5300 NIC	Office \ Unconstrained	7m x 4m	Single User				~1.4 m
Makki et al [30]	WiFi	TDOA	3x WARP boards	1 WARP board	Free Space	unknown	Single User				~1 m
Phaser [21]	WiFi	AoA	unknown	4x 5-element array Intel 5300 NIC	Indoor \ Unconstrained	2055 sq. ft.	Single User		~20°		~1m
SpotFi [27]	WiFi	AoA + TOF	WiFi APs	Intel 5300 NIC	Office \ Unconstrained	52m x 40m	Single User				40 cm
SWAN [48]	WiFI	AoA	Arduino Yun	2x 9-element switch array WPJ558 WiFi AP board	Office \ Unconstrained	600 sq. m.	Single User		2.6°		45 cm
ArrayTrack [47]	WiFI	AoA	Soekris box client	6x 8-element fully sync array WARP board	Office \ Unconstrained	unknown	Multi-User				23 cm
Monfared et al [31]	BLE	AoA	Ettus B205mini-i	2x 4-element array Ettus X310	Free Space	6m x 3m	Single User	~1°		14 cm (2m x 1m area)	
Qiu et al [34]	BLE	AoA	TI CC2640R2	3-element array TI CC2640R2	Free Space	unknown	Single User	~5°			
Dead on Arrival [15]	BLE	AoA	Ettus N200	2x 4-element (simulated) switched array Ettus B210	Office constrained	5m x 5m	Single User	~2°			95% <85 cm
Belloni et al [8]	BLE	AoA	Bluetooth beacon	16-element switched array	Free Space	50m x 40m	Single User				~80 cm
TyrLoc [22]	BLE	AoA	8-element switched array	2x 8-element switched array PlutoSDR + FPGA	Office constrained	105 sq. m.	Single User		2.9°		39 cm
This work	BLE	AoA	Phone	2x 8-element switched array PlutoSDR	Lobby \ Unconstrained Office \ Unconstrained	8.53m x 7.32m 9m x 8m	Single User Multi-User	3.4° 5.9°	2.37° 3.49°	36.4 cm 68.4 cm	27.4 cm 43.9 cm

methods are popular because of their low computational complexity and the fact that they can be retrieved from most devices. However, their tedious fingerprinting process and poor accuracy limit their usage to proximity-based applications. On the other hand, Time Difference Of Arrival (TDOA) and Time of Flight (TOF) approaches with WiFi [27, 30] and Ultra Wideband (UWB) [20, 37] provide high precision and can cover a large sensing area, but require special hardware with precise timing or synchronization and dedicated protocols to measure the time difference.

An alternative solution is the Angle of Arrival (AoA) based method, which can be obtained passively, like RSSI, by calculating the phase differences from synchronized antenna arrays [21, 47]. The AoA method provides high accuracy comparable to TDOA and TOF methods without the hardware and protocol limitations. In the case of BLE, the use of an RF switch simplifies the system's hardware, but requires special modification to the BLE packets [8, 15]. However, TyrLoc [22] is able to recover the target device's AoA without changing the packet structure and is realized with a single custom transmitter at a high packet transmit rate. Our work not only calculates the AoA without special modification to the BLE packet, but is also tested with multiple off-the-shelf BLE devices in real-world usage scenarios simultaneously, showing the possibility of large-scale deployment compatible with existing BLE-capable devices.

2.3 Performance Metrics and Baseline

Table 1 provides a summary of related work and highlights several important factors. One of the primary trends observed is that RSSI-based methods tend to cover larger test areas and utilize simple hardware but suffer from large localization errors. On the other hand, TDOA, TOF, and AoA approaches have relatively smaller test environments but can achieve sub-meter accuracy at the cost of specialized transmitters and receivers. Another key differentiator indicated in the table is the type of RF environment the system is tested in. Many systems perform better in constrained, free spaces where the transmitter and receiver are isolated from objects that can interfere with the RF signal, while other systems are optimized to work in multipath-rich environments. Additionally, only a few of the systems explore multi-device scenarios. Comparing this work to related work, it achieves comparable performance with other RF localization systems in both single-user and multi-user localization accuracy. Furthermore, this work is tested in a multipath-rich RF environment, uses off-the-shelf phones as transmitters, and is evaluated in a real-world usage scenario with users carrying the phone in their pockets.

3 SYSTEM OVERVIEW

This section provides an overview of the hardware components and the signal processing pipeline of the system, which are illustrated in Figure 2. Each processing block within the pipeline is detailed in subsequent sections of the paper. The proposed approach involves using a high-speed 8:1 RF Switch that sequentially connects each antenna to the input port of a single radio receiver chain. A stand-alone microcontroller commands the RF Mux to switch between antennas approximately every 30us, running freely in a pre-defined pattern without any communication with the receiver.

When a radio packet is received, it is sampled by multiple antennas sequentially, and the concatenated packet snippets are then demodulated into I and Q channels and sent to the computer via USB. While this approach reduces system cost and complexity by removing the need for synchronization hardware, it also poses a fundamental challenge where the system does not know which demodulated I and Q samples belong to which antenna. To overcome this issue, we observe that antenna switching events introduce discontinuities into the magnitude and phase of the demodulated waveform. Thus by having the microcontroller encode the antenna ID as variations in switch timing intervals, the system can monitor the discontinuities in software to recover both switch timing and the antenna ID.

To validate the proposed approach, the system was designed to receive and locate standard Bluetooth 4.0 packets transmitted by unmodified smartphones and mobile devices. The packet detection and identification method leverage the phase derivative information in the BLE Gaussian Frequency-Shift Keying (GFSK) modulation characteristics. This method outperforms traditional methods and is capable of processing the discontinuous waveform received by the switched antenna array. The antenna label is recovered during signal processing at the GNURadio C++ module level, which is device-independent and applicable to other SDRs. After retrieving the antenna label for the received packet samples, a synthetic virtual reference antenna waveform is generated, which is used to align the received packet snippets from each of the antennas in the array.

Finally, the customized Multi-Resolution Beaming and customized MUSIC algorithms output the received packet's Angle of Arrival (AoA) from the pseudo-synchronous antenna waveform. The signal processing pipeline requires no special modifications to the packets, such as an additional constant tone extension field at the end of the packet or unique bit patterns within the packet, and works with existing and already deployed BLE-compatible devices. The system achieves an average AoA error of 3.4° for moving targets with line-of-sight (LOS) conditions and 4.61° for non-line-of-sight (NLOS) cases where the BLE device, a smartphone, is carried in the user's pocket.

4 PACKET DETECTION AND IDENTIFICATION

Detecting and efficiently identifying the packet transmitted from the target BLE device out of heavy BLE traffic is crucial to the AoA system. Despite its importance, this process is often overlooked. Conventional methods for packet detection check the peak value or sudden changes in the received signal strengths (RSS). These methods, however, can be impacted by fluctuations in the RSS. The threshold might be too high for far-away devices with low transmission power or too low for noisy RF environments. The proposed approach leverages the unique phase derivative characteristic of BLE's gaussian frequency-shift keying (GFSK) modulation to detect and identify packets with high efficiency, even the receiving antenna switches in the middle of a packet reception. The following sections address the challenge of decoding BLE packets with the receiving antenna switching, then explain the phase derivative-based packet detection and identification implementation.

4.1 Challenge with Decoding BLE Packets

Figure 3a illustrates the received waveform on the advertising channel, with a 2 MHz sampling rate, centered at 2.402 GHz. An iPhone 12mini is transmitting at 30 advertising packets per second (pps) throughout the time frame. The plot shows two receivers - the receiver connected to a single antenna in green, and the receiver
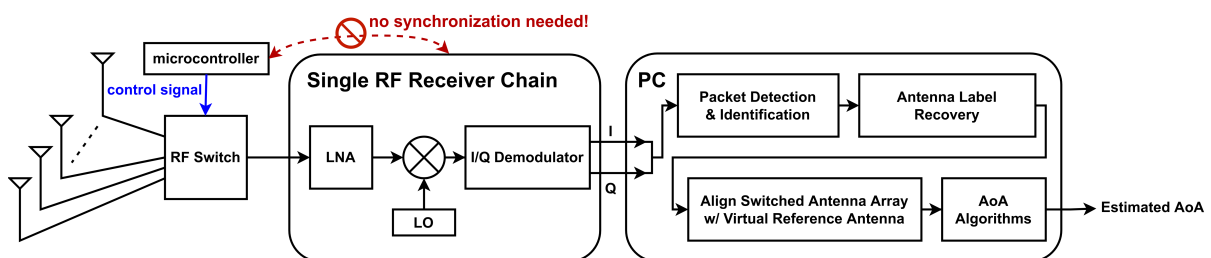

Fig. 2. System block diagram: An array of antennas are connected to an RF switch controlled by a microcontroller to switch between the antennas freely, unsynchronized with the RF receiver. The output of the RF switch connects to a single RF receiver chain, and the raw IQ samples of the downconverted waveform is then sent to a computer. The software processing pipeline on the computer first performs packet detection and identification to extract the packet. Then, the antenna used to receive each sample in the packet is recovered. The packet waveform is aligned with a virtual reference antenna to compensate for carrier frequency offset. Finally, the packet's angle of arrival is calculated as the output of the system.
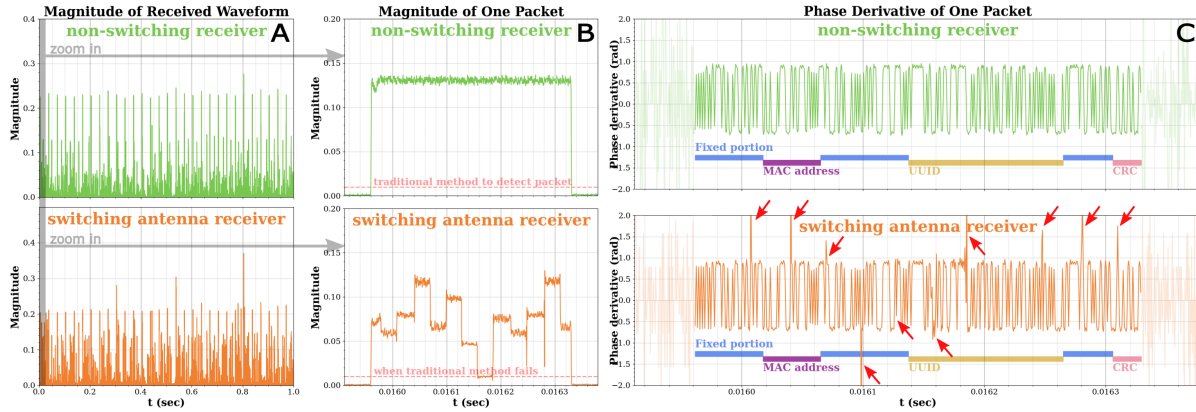
Fig. 3. The figure on the left shows the received magnitude from a non-switching antenna receiver in green and a switching antenna receiver in orange. The middle figure zooms into one packet. The red lines show the traditional magnitude threshold method to detect the arrival of a packet, which does not work with the switched antenna array. The right figure shows the received packet's phase derivative waveform. The spikes pointed out with red arrows in the switched antenna waveform in orange indicate the places of potential bit errors that might occur during decoding. The packet-dependent information such as MAC address is in purple, UUID is in yellow, and CRC is in pink, while the other fixed portions are in blue.

connected to an RF switch switching through 8 antennas in orange. Each spike in the magnitude waveform represents an advertising packet in the BLE traffic. Figure 3b zooms in on an advertising packet transmitted from the iPhone 12mini following the iBeacon protocol. The received magnitude jumps high when the packet arrives and returns to the noise floor afterward for the non-switching receiver. For the switching antenna receiver, some antennas might have low RSS, and RSS spikes occur at switching edges, making it challenging to set a fixed threshold for packet detection. To decode the packet, the phase derivative of the packet is calculated as shown in Figure 3c by subtracting the phase measurement of the current sample from that of the previous sample. The transmitted bits can be easily recovered by checking the sign of the phase derivatives for the non-switching receiver's waveform. However, the switching antenna receiver introduces bit errors with irregular spikes in the phase derivative waveform, highlighted with red arrows in Figure 3c. As a result, even if the packet passes the detection stage, it fails the cyclic redundancy check (CRC), making it necessary to explore alternative packet detection and identification methods for the switching antenna receiver.

4.2 Phase Derivative Based Packet Detection and Identification

An alternative method for detecting and identifying BLE packets transmitted from target devices can be achieved by utilizing the unique characteristic of phase derivative in BLE's GFSK modulation. BLE beacons transmit device-specific information, such as MAC address and UUID in the payload, to nearby receivers for identification. Different packet payload also changes the CRC bits at the end of the packet. Before sending the packet, the payload is whitened to generate a balanced bit sequence according to the BLE standard. The whitening process is local, meaning a one-bit change in the payload will only affect the same bit at the output. The whitened bits are then encoded in the transmitted waveform through GFSK modulation, which can be visualized in the waveform's phase derivative. For iBeacon-type packets under the same settings, all packets have the same phase derivative waveform except for the MAC address, UUID, and CRC sections. The phase derivative waveform of an iBeacon packet structure is shown in Figure 3c, where the MAC address section is highlighted in purple, the UUID section in dark yellow, the CRC section in pink, and the rest in blue. This insight enables a new method of packet detection and identification.

The correlation score between the phase derivative of an ideal iBeacon packet and the received phase derivative is calculated for the non-changing portion of the waveforms for packet detection. The ideal iBeacon waveform is generated from Matlab's BLE toolbox, and the phase derivatives are set to zeros at places outside the blue portions in Figure 3c. If the correlation score is above a threshold (0.5 through empirical results), an iBeacon packet is detected. The UUID portion's phase derivative is then extracted from the detected packet and correlates with the ideal phase derivative's UUID portion. If the highest score is the only one that is above the threshold (0.5 through empirical results), the received packet is successfully identified. The UUIDs are entirely randomized following the BLE protocol, so the packet detection and identification methods work with any iBeacon-compatible devices.
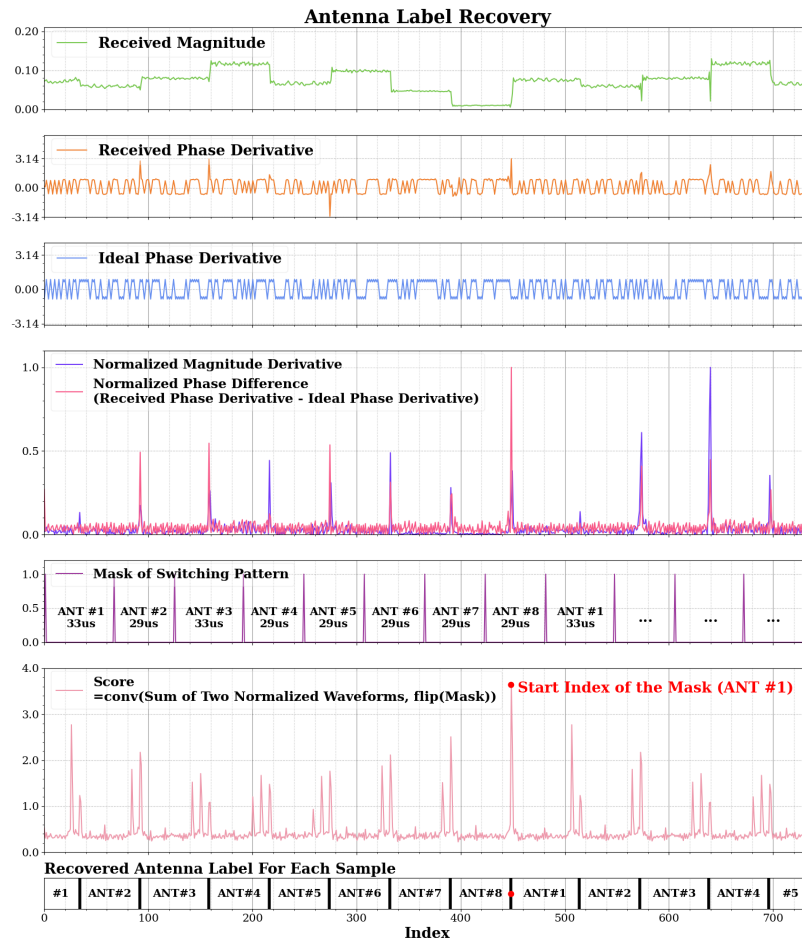

Fig. 4. To recover the antenna used to receive each sample, the irregularity (spikes and jumps) in both magnitude and phase are harvested. The normalized magnitude derivative in purple is calculated from the received magnitude in orange. The normalized phase difference between the received and ideal waveform's phase derivatives is highlighted in pink. The sum of the two normalized waveforms is convoluted with the mask of the switching pattern to find the best possible location for the pattern. The recovered antenna labels for each segment of the samples are at the bottom.

5 ANTENNA LABEL RECOVERY

Switched antenna arrays reduce the number of receivers and lower the system's complexity and hardware cost compared to fully synchronized arrays. However, tracking which antenna is used to receive each sample requires additional resources, such as an extra receiver recording the RF switch status or modifying the SDR firmware to have a custom interface with the RF switch. The proposed method offers a solution by using an external microcontroller to control the RF switch without communication with the receiver. The antenna labels for the received samples are retrieved at the GNURadio C++ module level, providing cross-SDR portability for realizing switched antenna arrays.

Switching the receiving antenna from one to another in the middle of receiving a packet creates jumps and spikes in the received magnitude and phase derivative waveforms, as depicted in green and orange in Figure 4. By varying the receiving time of each antenna controlled by the RF switch, the antenna used to receive a segment of samples can be identified through the unique spacing between the edges of the waveform. Instead of searching for jumps in the raw magnitude waveform, the waveform's magnitude derivative is used, shown as light purple in Figure 4. With the packet already identified using the phase derivative method outlined in Section 4.2, an ideal waveform for the packet can be generated, with its phase derivative depicted in blue in Figure 4. The jumps in the received phase derivative can be found by subtracting the ideal waveform's phase derivative. The difference between the received and ideal phase derivatives is then normalized to highlight the jumps, shown in pink in Figure 4. The sum of the normalized magnitude derivative waveform and the phase derivative's difference waveform forms a feature waveform. The feature waveform is then convoluted with a mask, created with ones when the receiving antenna switches and zero elsewhere according to the switching pattern. The mask is shown in dark purple, and the convolution score is shown in light pink in Figure 4. The peak index in the final score determines the starting indexof the mask pattern, and the antenna label for each sample can be found by shifting the mask to the peak index, as demonstrated at the bottom of Figure 4. The peak index in the final score determines the starting index of the mask pattern. The antenna label for each sample can be recovered by shifting the mask to the peak index, as shown at the bottom of Figure 4. This process enables the system to identify the antenna used for each sample without modifying the receiver's firmware to synchronize with the RF switch.

Significant differences in the spacing between the jumps in the waveform help to encode and extract the antenna labels and switch timing more easily. However, antennas with fewer samples are more prone to corruption from noise, which impacts the system's accuracy in AoA calculation. On the other hand, having samples from every antenna in the array increases the diversity of the input information for more accurate AoA calculation. Therefore, the switching pattern has to at least switch through all antennas within a single packet and has a balanced receiving time on each antenna. Our chosen pattern stays on antennas 1 and 3 for 33 us and the rest of the antennas for 29 us, switching through the antenna array 1.5 times within a packet reception period. Antennas that appear twice will be used to create the virtual reference antenna's waveform, which will be discussed in the next section.

6 ALIGNING SWITCHED ARRAY WITH VIRTUAL REFERENCE ANTENNA

Mimicking an N-element antenna array using an RF switch with a single receiver chain creates a switched antenna array, reducing the complexity and cost of the system significantly. The main challenge of using a switched antenna array is the carrier frequency offset (CFO) between the transmitter and receiver. Existing solutions switch back and forth between an anchor antenna and the rest of the antennas to estimate CFO for every phase difference measurement. To compensate for the CFO, the proposed method only visits all antennas once, switching antennas (N+1) times instead of (3N-3) times with the help of the virtual reference antenna. In this section, we present the concept of a virtual reference antenna and demonstrate how it can be used to align
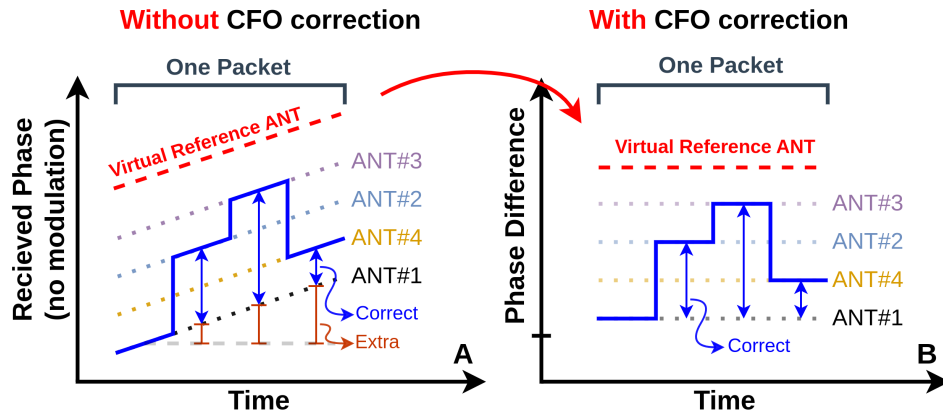
Fig. 5. Switched antenna array receives segments of the packet with different antennas sequentially. The slanted, **unmodulated** received phase caused by carrier frequency offsets is highlighted in blue on the left. Extra phase rotation skews the phase difference measurement of each antenna pair highlighted in brown. With the help of a virtual reference antenna waveform created by rotating the ideal waveform of the packet, the de-rotated phase difference can be calculated and is colored blue on the right. However, the slope in the received phase is disguised while the waveform is modulated (as shown in Figure 6). The use of the modulated virtual reference antenna waveform not only helps uncover the modulated received phase into the blue line on the right but also aligns the phase difference for all antennas.

the switched antenna array in a real-world scenario. In this section, we first address the issue caused by the CFO when using a switched antenna array and propose a novel solution to overcome this problem by creating a virtual reference antenna waveform.

6.1 Pseudo Synchronous Array with Virtual Reference Antenna

The hardware variations across manufacturers and the changes in the environment, such as temperature and humidity, result in a slight frequency difference between the oscillators in the transmitter and the receiver called carrier frequency offset (CFO). Another frequency difference in the sampling frequency called sampling frequency offset (SFO) exists and has the same effect as the CFO in the single carrier frequency modulated waveform used case. For simplicity, we use the term CFO as the combination of CFO and SFO in the following text. The CFO's existence adds a cumulative phase rotation to each received sample, as shown in blue in Figure 5a. Thus, the phase difference between each antenna pair calculated from the blue line is skewed. This is not a problem with synchronous antenna arrays since all antennas are received simultaneously. The 4 dotted lines in 5a are captured with a synchronous array, so the additional phase rotation cancels out during the calculation.

Instead of having a receiver for each antenna forming a synchronous array, having one virtual non-switching receiver creates a baseline, highlighted red in Figure 5a. Under this configuration, two antennas are received at once at any given period, creating a 2-element virtually synchronous array. The correct phase difference is then extracted by subtracting the received phase from the phase of the virtual reference antenna. Figure 5b shows the unskewed phase difference between the antennas. A pseudo synchronous array is formed and aligned without deploying an actual reference antenna. In the real world, the received BLE packet is GFSK modulated, so the received phase is no longer a tilted straight line. A modulated ideal waveform is introduced in the following section as the virtual reference antenna for real-world implementation.
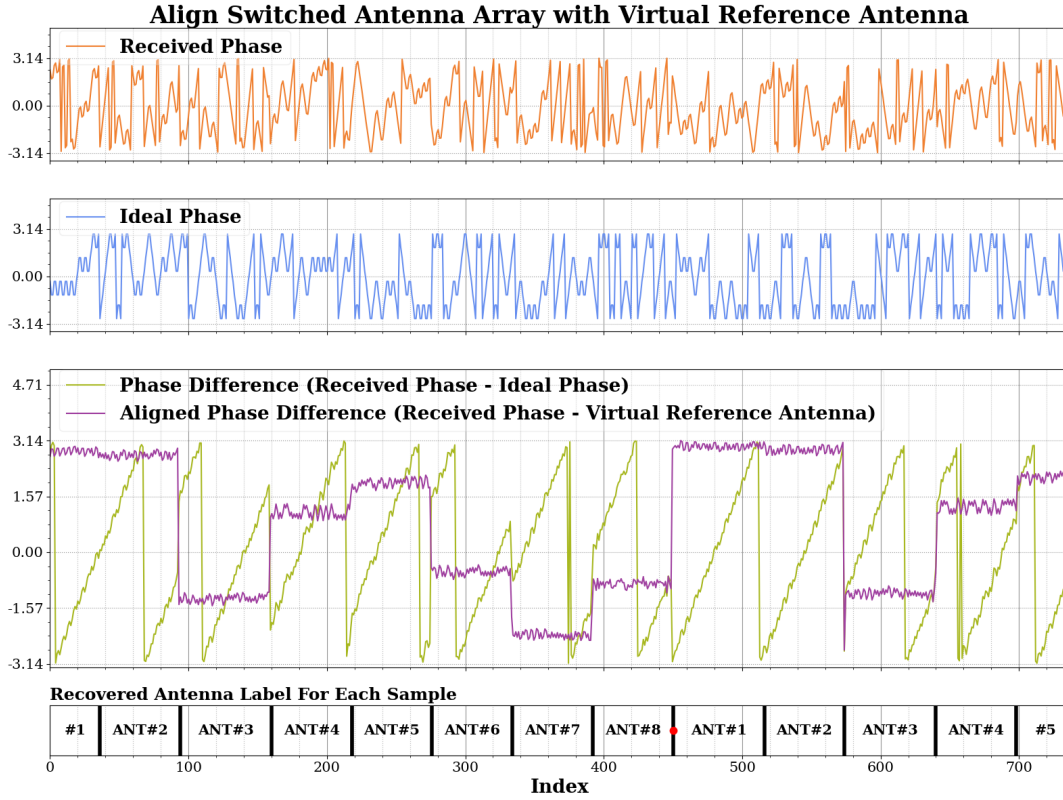
Fig. 6. After the packet is identified, the ideal waveform in blue is created with the known bits of the packet. The phase difference of the received and ideal waveform in green reveals the slope caused by carrier frequency offset, which is unretrievable without the help of the ideal waveform. The system estimates each antenna segment's slope and rotates the ideal phase to create a virtual reference antenna. The aligned phase difference is in purple, same as the concept in Figure 5.

6.2 Compensating CFO with Ideal Waveform as Virtual Reference Antenna

Figure 6 shows the process of constructing the virtual reference antenna waveform. The received phase of a BLE packet from the switched array is colored orange in Figure 6. The slope introduced by the CFO is hidden in the received phase since the packet is GFSK modulated. The ideal phase is generated from Matlab's BLE toolbox with the known bits identified in Section 4 as the virtual reference antenna's waveform. By subtracting the two, the CFO slope is revealed in the phase difference waveform, highlighted green in Figure 6. Since the phase difference waveform breaks continuity at switching edges, the recovered antenna labels from Section 5 are used to locate the edges and remove them during the calculation. The system then rotates the ideal phase based on the CFO slope estimation in each segment and calculates the aligned phase difference, highlighted purple in Figure 6. A second step checks if the phase differences of the separate segments received from the same antenna are at the same level and fine-tune the CFO. The designed switching pattern mentioned in Section 5 switches through the antenna array 1.5 times within a packet, providing at least one antenna to receive two packet segments for the fine-tuning CFO operation. Finally, the phase difference is aligned to the same level and free from the CFO skew. The creation of the virtual reference antenna with the ideal waveform converts a switched antenna array into a pseudo synchronous array, allowing the system to perform AoA calculation with the correct phase measurements, as described in the next section.

7 ANGLE OF ARRIVAL CALCULATION

The pseudo synchronous antenna array aligns the phase of each receiving antenna with the help of the virtual reference antenna. Since the system only receives segments of the signals from different antennas, typical AoA algorithms need to be modified to fit the case. This section explores two algorithms to estimate the AoA of the signal under the asynchronous array configuration.

7.1 Multi-Resolution Beaming

Once the waveform of the virtual reference antenna is reconstructed with recovered antenna labels, relative phase measurements of each antenna of the switched antenna array (SAA) can be extracted, which can further be used for AoA estimation. Let the aligned SAA captured and virtual reference waveforms be $\mathbf{x}_0$ and $\tilde{\mathbf{x}}_r$. From the antenna labels, the waveforms can be divided into sub-packets of each antenna, denoted as $\mathbf{x}_0^{(m)}$ and $\tilde{\mathbf{x}}_r^{(m)}$ for the antenna m. Then, the phases of each antenna can be obtained relative to that of the virtual reference as below,

$$\mathbf{\Psi}^{(m)} = \text{angle} \left(\frac{\mathbf{x}_0^{(m)}}{\tilde{\mathbf{x}}_r^{(m)}} \right) \tag{1}$$

Then, the relative phases between antennas can be utilized to infer the gap of time-of-arrival, which is associated with the angle of arrival θ, assuming that the transmitter is far from the antenna array,

$$\mathbf{\Psi}^{(m_1)} - \mathbf{\Psi}^{(m_2)} = 2\pi \left(\frac{d(m_1 - m_2)}{\lambda} \sin(\theta) + k \right) \tag{2}$$

where d is the gap between antennas and k is an integer introduced due to the circular periodicity of the angle. The inferred AoA has different resolution and uncertainty depending on the gap between antennas, and a straightforward way to estimate the AoA is to combine the contributions of all the pairs together [41], which is investigated as a multi-resolution beaming (MRB) scheme for performance evaluation.

7.2 Modified MUSIC with Asynchronous Array

MUSIC method has shown excellent performance for AoA estimation from antenna array systems [31, 43, 46], where the pseudo spectrum is obtained from the noise subspaces, extracted by eigen-decomposition of the correlation matrix [38],

$$\mathbf{R}_{xx} = \frac{1}{N} \mathbf{X}\mathbf{X}^H \tag{3}$$

where $\mathbf{R}_{xx}$ is the sample auto-correlation matrix and $\mathbf{X} = [\mathbf{x}_1 \ \mathbf{x}_2 \ \dots \ \mathbf{x}_M]^T$ is the $M \times N$ matrix of M antenna waveforms of N samples. From the eigenvectors $\{\mathbf{v}_1, \mathbf{v}_2, \dots, \mathbf{v}_M\}$ sorted in decreasing order, the MUSIC pseudo-spectrum is

$$\hat{P}_{MU}(\theta) = \frac{1}{\sum_{i=p+1}^M |\mathbf{a}(\theta)^H \mathbf{v}_i|^2} \tag{4}$$

where $\mathbf{a}(\theta) = [1 \ e^{j(2\pi d/\lambda)\sin(\theta)} \ \dots \ e^{j(2\pi(M-1)d/\lambda)\sin(\theta)}]^T$ is the beam steering vector for angle θ, and p is the number of signal sources. Note that $\hat{\mathbf{R}}_{xx}$ in (3) is obtained from simultaneously captured waveforms from multiple data channels in general. For applying MUSIC for AoA estimation from SAA systems, where individual antenna waveforms are sequentially captured at different times, a virtual synchronization scheme is introduced [22]. In this approach, antenna is switched after a packet received with a predefined order, for example $\mathbf{x}_1, \mathbf{x}_1, \mathbf{x}_2, \mathbf{x}_1, \mathbf{x}_1, \mathbf{x}_3, \dots, \mathbf{x}_1, \mathbf{x}_1, \mathbf{x}_M$ to estimate the phase shifts by CFO $\{\phi_{m1}\}$, relative to the virtual pivot antenna $\left\{ \hat{\mathbf{x}}_1^{(m)} \right\}$, predicted from $\mathbf{x}_1$s ahead of $\mathbf{x}_m$. Then, the virtually synchronized waveforms by adjusting the phase shifts $\left\{ \mathbf{x}_m e^{-j\phi_{m1}} \right\}$ can be obtained for estimating sample auto-correlation in (3), and AoA estimation by MUSIC

in (4) can be applied. Note that the CFO adjusted waveforms $\left\{\mathbf{x}_m e^{-j\phi_{m1}}\right\}$ are effectively synchronized, since each antenna observes the full packet of same data patterns at different times.

However, for the system proposed in this paper, antenna waveforms are captured not only at different times with CFOs but also from different data patterns due to in-packet switching. For virtual synchronization of the antenna waveforms, the CFO compensated reference antenna waveform $\tilde{\mathbf{x}}_r$ is used and a set of synchronized antenna waveforms are synthesized in sub-packets as below,

$$\tilde{\mathbf{x}}_m^{(i_s)} = \mathbf{x}_0^{(m)} \frac{\tilde{\mathbf{x}}_r^{(i_s)}}{\tilde{\mathbf{x}}_r^{(m)}} \tag{5}$$

where $\mathbf{x}_0^{(m)}$ and $\tilde{\mathbf{x}}_r^{(m)}$ are sub-packets of the received and virtual reference waveforms, corresponds to the antenna m. The fraction of sub-packets of $\tilde{\mathbf{x}}_r$ in the right-hand side of (5) effectively changes the data patterns of the sub-packets m to that of the i_s with preserving the phase errors. By concatenating the $\tilde{\mathbf{x}}_m^{(i_s)}$ for $i_s = 1$ to M, the waveforms of antenna m can be synthesized for all-antenna length $L = \sum_{i_s=1}^{M} l_{i_s}$ with corresponding data patterns. Note that the lengths of sub-packets $\{l_i\}$ are not equal for all the antennas as commented in Section 5, and sub-packet synthesis in (5) may need extra padding or truncating to keep the length of the i_sth sub-packet. This enables us to get a set of M virtually synchronized antenna waveforms for near the packet length from a single packet observation. Then, MUSIC-based AoA estimation can be obtained from the synthesized sample auto correlation. Figure 7 illustrates the phase of the synthesized waveforms of antenna 1, 2, 3, and 8 relative to the virtual reference $\tilde{\mathbf{x}}_r$. The measured relative phases of the antennas are expressed by the thick lines, which are repeated for different sub-sections by the virtual synthesis step in (5). Thus, all the synthesized waveforms have
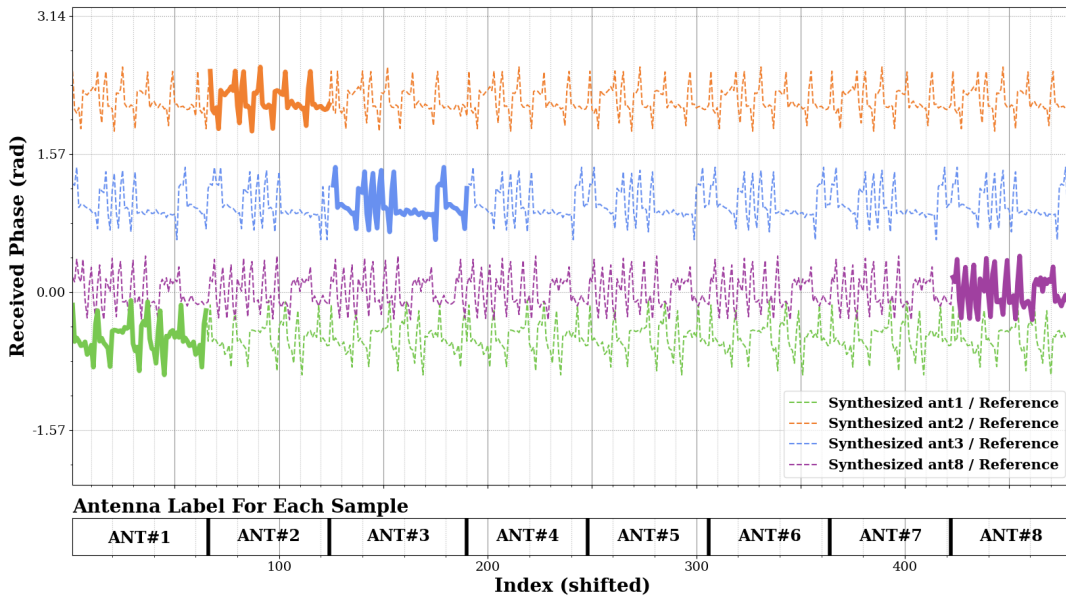

Fig. 7. Phase difference between the synthesized waveforms of the switched antenna array and the virtual reference antenna. The solid line segments are each antenna's actual received phase error patterns. The patterns are duplicated onto the ideal waveform to synthesize the full waveform of each antenna. The synthesized waveforms can be processed by MUSIC to estimate the AoA of the signal.
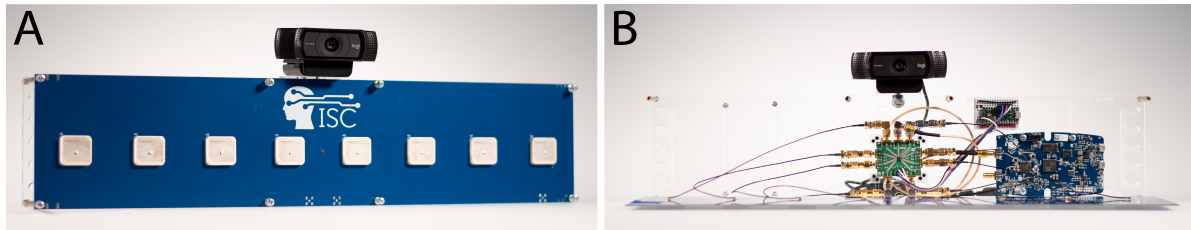
Fig. 8. (a) The front of the antenna array with 8 patch antennas of 6.24 cm spacing. (b) The inside of the switched antenna array, with a 8:1 RF switch at the center, a Teensy 4.0 microcontroller on the top right, and a PlutoSDR on the right all mounted on a acrylic back plate. The Teensy is powered by the PlutoSDR, but is not synchronized with it.

phase shifts with random fluctuations from the same reference waveform, and can be regarded as effectively synchronized measurements for MUSIC analysis.

8 EVALUATION

Multiple experiments have been conducted to evaluate different aspects of the system. This section outlines 1) the hardware utilized for the evaluation of the system, 2) examines the 1-dimensional Angle-of-Arrival (AoA) estimation and 2-dimensional localization accuracy under optimal conditions in a low-multipath environment, and 3) presents the real-world evaluation of the system in a multipath-rich office space.

8.1 Switched Antenna Array Hardware

The design of the switched antenna array receiver is depicted in Figure 8. The front of the array comprises eight PulseLarsen W3229 patch antennas that are soldered onto a printed circuit board (PCB) that also includes a ground plane for the patch antennas. The antennas are spaced 6.24 cm apart, which is half the wavelength of the 2.402 GHz carrier frequency used for BLE's advertising channel 37. The antennas are connected to an EV1HMC253AQS24 RF switch, which is mounted in the center of a acrylic back plate. The switch is controlled by a Teensy4.0 microcontroller located on the top right corner of the plate via three general-purpose input/output (GPIO) pins. The RF switch is switched at pre-defined intervals, as described in Section 5. The output of the RF switch is connected to the receiver, a PlutoSDR, which collects RF samples at a rate of 2 MHz. The PlutoSDR
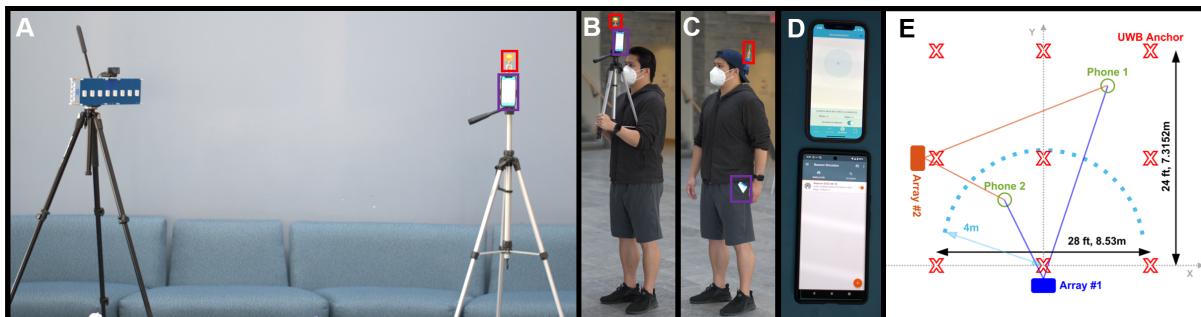

Fig. 9. (a) The test setup for a stationary target where the phone is broadcasting BLE packets on a tripod 4m away from the switched antenna array. (b) The best case while a user moves around and holds the tripod with the phone on top, always having non-blocking LOS to the receiver. (c) The real-world case while a user moves around with the phone in the pocket. The UWB tag in red is used for ground truth collection. (d) The iBeacon simulator app running on an iPhone 12mini (top) and a Pixel6 Pro. (e) The floorplan of the test area. The two switched antenna arrays are in blue and orange, the UWB anchors are in red X's covering a 8.53 m x 7.32 m test area.
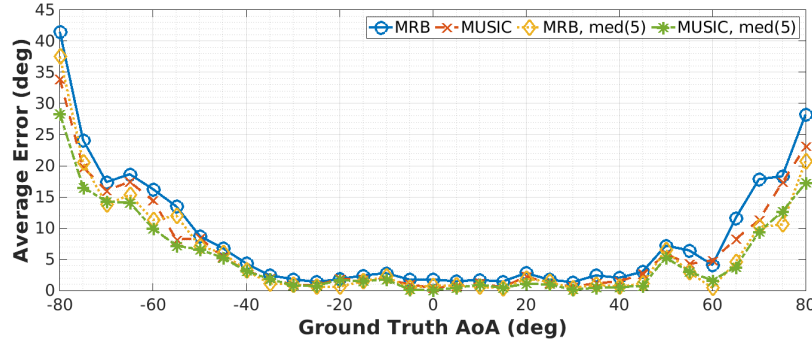
Fig. 10. Ground truth angle versus median error. The AoA accuracy is low within ±60 degrees of AoA and increases as the ground truth AoA increases, which aligns with the patch antenna's gain pattern and the natural characteristic of the linear antenna array.

provides power to the Teensy and the RF switch, but does not control them, enabling the integration of any single port receiver into the system. The samples collected by the PlutoSDR are sent to a computer via a USB cable for real-time identification of BLE packets and calculation of AoA. The computer is equipped with an Intel Core i7-8700 CPU and 32 GB of RAM.

The transmitter broadcasts iBeacon-type BLE advertising packets at a rate of 30 packets per second using a commercially available beacon simulator app. Figure 9d illustrates the use of the simulator app on both Android (Pixel6 Pro at the top) and iOS (iPhone 12 mini) devices. The MAC addresses and the UUIDs are entered into the system for whitelisting. The latency of the system is estimated to be less than 4 ms, as it takes 3.56 ms to process a packet.

8.2 Technical Evaluation

Experiments to evaluate the fundamental aspects of the AoA estimation performance are carried out in a low-multipath lobby environment to test the system's upper limit. This section evaluates the angular accuracy with a stationary target and the 1D and 2D accuracy of moving targets with line-of-sight (LOS) and non-line-of-sight (NLOS) conditions.

8.2.1 Experiment Setup. An 8.53 m x 7.32 m area (672 sq. ft.) in a lobby with no objects within the perimeter is used as a low-multipath environment to evaluate the system. An ultra-wideband (UWB) localization system capable of tracking UWB tags at 100 Hz is installed in the test area to collect ground truth data. The red Xs in Figure 9e show the locations of 9 Chialos DWUSB UWB anchors. Antenna array #1 at the bottom edge of the figure and antenna array #2 at the left edge are both on tripods 1.5m off the ground facing toward the test area and are marked in blue and orange in Figure 9e.

8.2.2 Angular Accuracy with Stationary Target. Figure 10 shows the average error of Multi-Resolution Beaming (MRB) and MUISC at each ground truth angle. In this test, the transmitter is placed 4m away from the receiver at angles from -80~80 degrees with a 5-degree step as the dashed line highlighted in light blue shown in Figure 9e. Ten seconds of data is collected at each angle with the transmitter mounted on a tripod 1.5m off the ground, as shown in Figure 9a. The average AoA estimation error is between 1~5 degrees within ±40 degrees of AoA and below 10 degrees within ±60 degrees of AoA. The results are aligned with the expectation as the uniform linear antenna array performs best at the center, and the accuracy drops when the source is at large angles. Furthermore, the gain of the patch antenna drops around 6 dB at ±60 degrees of AoA compared to the center [1].

For applications in the real world, the antenna arrays are likely to be mounted on ceilings or up on the walls facing downwards, locating devices at a distance within the ±60 degrees range. The median filter with a length of 5 reduces the error by removing the jitter at the output. The stationary target evaluation provides a baseline measurement of the system's abilities and limitations, laying the foundation for the more challenging scenario for tracking a moving target in the following section.

8.2.3 AoA Estimation Accuracy with Moving Target. While a stationary target with no movement in space creates a static, low-noise RF environment for the radio waves to travel, adding movements to the target creates dynamic multipath between the transmitter and the receiver. Additionally, the line of sight between the receiver and the device may be partially or completely obstructed, negatively affecting the system's performance when a user carries the device.

In the first scenario, the transmitter always has a line of sight (LOS) to the receiver. For this best case, data is collected in four sets, each 5 minutes long. The phone, acting as the transmitter, is mounted on a tripod with a UWB tag behind it. A person holds the tripod above their chest, maintaining LOS between the phone and receiver. The person walks and stops randomly during the test, as shown in Figure 9b. The estimated AoA for the first set is shown in Figure 11a, calculated using MRB and MUSIC with a median filter of length 5. The results are colored blue and yellow, respectively, with the ground truth in red. MRB has more jitter, resulting in a higher AoA error, but a lower median error than MUSIC. The average AoA error is 3.71° for MRB and 3.44° for MUSIC. The CDF of both methods in the best case is shown in Figure 12. MUSIC performs better, with a median error of 2.37° compared to MRB's 2.43°. Both methods have 95% of their errors below 10 degrees, demonstrating the system's reliability in estimating AoA in LOS situations.

The second scenario involves carrying the phone in the user's pocket, which is the most common place for keeping a phone as illustrated in Figure 9c. This practical yet challenging usage scenario is not typically reported or demonstrated. The user wears a custom-made UWB hat to gather ground truth data. The phone is placed against the user's thigh, causing the BLE signal transmitted from the phone to be constantly weakened. When the user turns and faces away from the antenna, completely blocking the receiver's line of sight, the RF environment becomes even more challenging. Three sets of data, each lasting 5 minutes, are collected with the phone in the user's pocket. Figure 11b displays the estimated AoA with the phone in the pocket. When the pocket with the
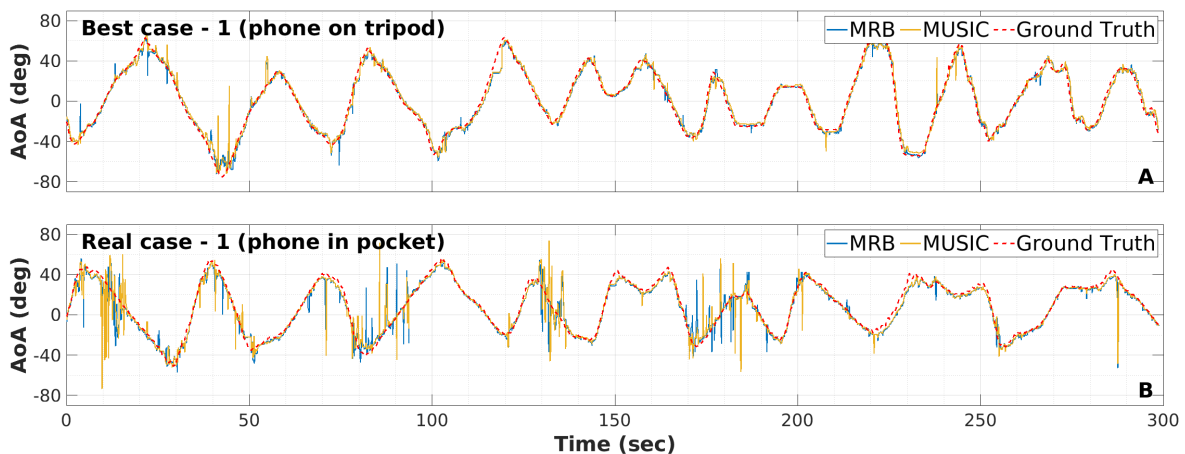

Fig. 11. (a) The AoA trace for the best case where the user carries a tripod with the phone on top for 5 minutes. The blue and yellow lines are the output of the system, and the ground truth is in red.(b) The AoA trace for the real-world case where the user carries the phone in the pocket for 5 minutes.

Table 2. AoA Estimation Error from Moving Target

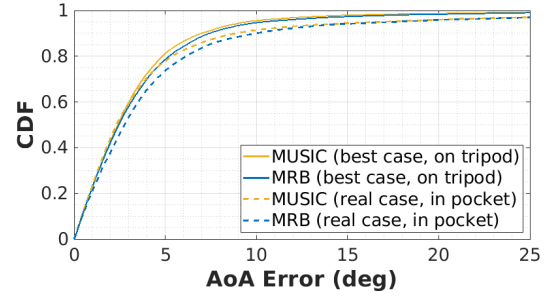| Scenario		Single packet		Median of 5	
		MRB	MUSIC	MRB	MUSIC
Best case (Phone at tripod)	Average	5.89°	5.14°	3.71°	3.44 °
	Median	2.89°	2.66°	2.43 °	2.37°
Real case (Phone in pocket)	Average	8.41°	7.65°	5.03°	4.61°
	Median	3.24°	2.65°	2.77°	2.33°

Fig. 12. CDF of AoA estimation error for moving target.

phone is facing the antenna array, the system is able to calculate the AoA with the same level of performance as the best case. However, when the user turns, facing the pocket and phone away from the antenna array, both MRB and MUSIC have larger errors in estimated AoA. The average error for MRB is 5.03° and 4.61° for MUSIC. The CDF for the in-pocket case is represented by dash lines in Figure 12 and shows a median error of 2.77° for MRB and 2.33° for MUSIC. The AoA error is less than 10 degrees for 90% of the data with both AoA methods. The accuracy of P2 is lower than P1 because P2 is moving at a faster pace. The result shows that the system's AoA estimation is not only accurate but also consistently within close range to the true angle. Table 2 summarizes the AoA estimation errors.

8.2.4 Localization Accuracy. With two antenna arrays at separate locations in the space, the system can recover the user's 2D location at the intersection of the two AoA estimation lines. The system locates the device in 2D and smoothes the output with a Kalman filter. Figure 13a and 13b shows the 2D traces for best case when the phone is on a tripod within the antenna array's LOS. Figure 13c and 13d shows the 2D traces while the phone is in the user's pocket. A second device is on a second user during the 3rd dataset of the in-pocket used case. The other trace in green and purple shows the localization result of the second device, demonstrating the system's capability to locate multiple phones simultaneously. For the best case, the average error is 38.2 cm for MRB and 36.4 cm for MUSIC. The in-pocket case has a slightly larger average error of 42.3 cm for MRB and 40.4 cm for MUSIC. The CDF for the localization performance is shown in Figure 14. Localization errors are summarized in Table 3.

Using commercially available phones without any modifications to their advertising packets, transmission rates, or transmitter power ensures that the system operates in realistic usage scenarios. This allows tracking
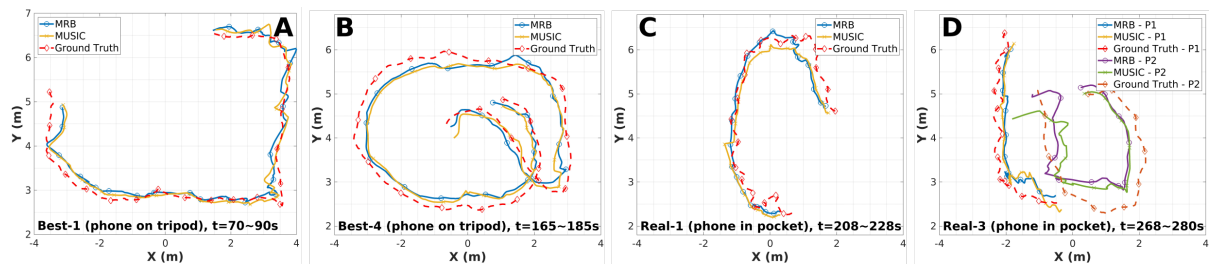

Fig. 13. (a)-(b) The 2D traces of the best case where the user carries a tripod with the phone on top. The blue and yellow lines are the system's output, and the ground truth is red. (c)-(d) The 2D traces for the real-world case where the user carries the phone in the pocket. A second user with a second phone in the pocket joined in (d).

Table 3. Localization Error from Moving Target

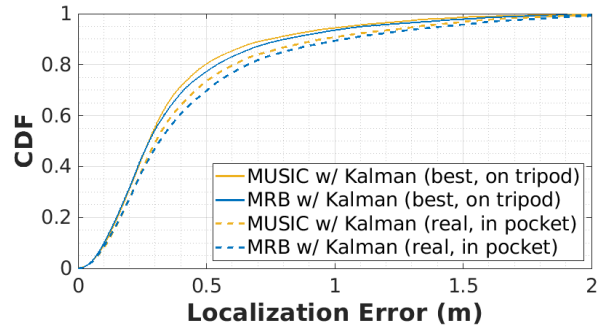| Scenario		MRB	MUSIC
Best case (Phone at tripod)	Average	38.2 cm	36.4 cm
	Median	27.6 cm	27.4 cm
Real case (Phone in pocket)	Average	42.3 cm	40.4 cm
	Median	31.1 cm	30.9 cm

Fig. 14. The CDF of localization error for moving target.

multiple targets even in environments with a high density of BLE devices in range. The following section presents the results of a real-world test that tracks multiple users simultaneously in an office environment.

8.3 Real-World Evaluation

The system's performance is further tested in an office space with various objects creating a multipath-rich environment. This section focuses on analyzing the impact of the user's interaction with the BLE device on the AoA estimation, as well as the 1D and 2D localization accuracy in both single and multi-user scenarios.

8.3.1 Experiment Setup. A 9m x 8m office space (775 sq. ft.) was used to evaluate the system's performance in a multipath-rich environment as shown in Figure 15. The office space contained various objects such as 17 desks, 18 chairs, 8 computers, and 12 monitors that interfere with RF signals. Two antenna arrays were placed 1.35 meters off the ground, one at the left and one at the bottom of the space, as shown in Figure 15c. Each participant wore a custom hat with a Vive Tracker 3.0 attached, which was tracked at 60Hz by 4 SteamVR base stations 2.0 at the four corners of the area. The ground truth data collected included a time stamp, a 3x3 rotation matrix, and the XYZ coordinates of the tracker. During the experiment, the participants were free to move around the space, work at their desks, and engage in conversations with others with a phone transmitting BLE packets in their pockets.
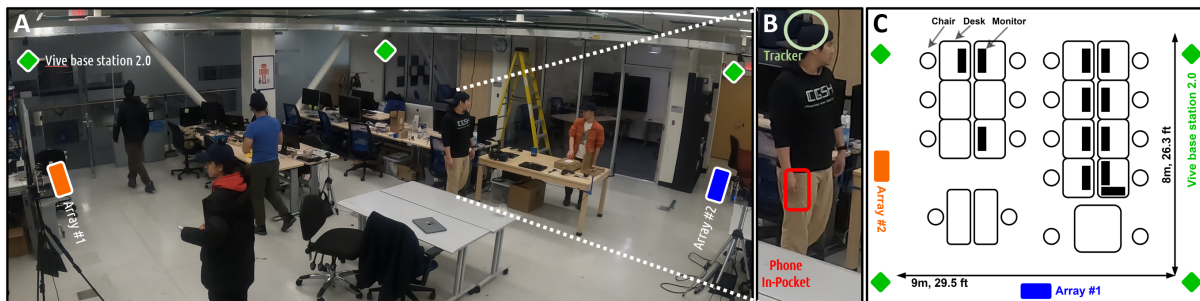

Fig. 15. (a) The multipath-rich office space environment with desks, chairs, and monitors. 4 Vive base stations are deployed to record the groun truth while 5 users wear a hat attached with a vive tracker. The phone is in the user's pocket tracked by 2 antenna arrays on the side. (b) A user with the tracker on the hat and the phone in his pocket. (c) a top down view of the testing environment.
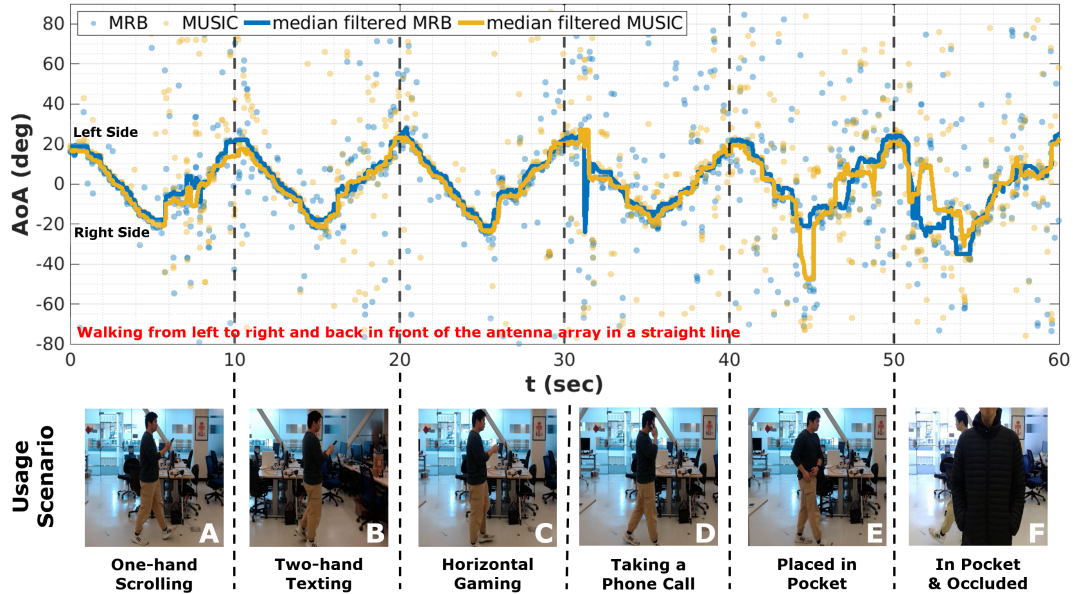
Fig. 16. The AoA estimation results under 6 different usage scenarios with the user walking in front of the antenna array from left to right and back for each scenario. (a) The user is scrolling the phone with one hand. (b) The user is texting with both hands. (c) The user is gaming horizontally with both hands. (d) The user is taking a phone call. (e) THe user carries the phone in the pocket. (e) The user carries the phone in the pocket with a second user blocking the LOS. Results show the system can estimate the AoA robustly under different conditions.

8.3.2 User's Impact on AoA Estimation. In real-life scenarios, people use their phones in various ways, not just by carrying them in their pockets. This can lead to obstructions in the line-of-sight (LOS) between the phone and antenna array, resulting in poor AoA estimation. Figure 16 illustrates the AoA estimation over time as the user interacts with the phone in six different ways while walking from side to side in front of the antenna array. The conditions include scrolling through a news feed (A), typing with two hands (B), gaming in a horizontal position (C), answering a call (D), carrying the phone in a pocket (E), and carrying the phone in a pocket with another person obstructing the LOS (F).

The median-filtered AoA traces follow the user effectively in sections A to C, demonstrating the robustness of the system when the phone is partially obscured by the user's hand. In sections D and E, when the user answers a call with the phone against their head or carries the phone in their pocket, the RF signal is weakened and blocked by their body, creating a more complex RF environment and leading to a more scattered raw AoA estimation in Figure 16. Finally, the presence of a second person blocking the first user's LOS in section F causes significant fluctuations in the raw AoA estimation and large jumps in the median-filtered AoA traces. These results indicate that the more the device is obscured by the user, the less stable the raw AoA estimation becomes. Particularly, the LOS blocking by other users presents a significant challenge to the system, which is further discussed in Section 8.3.4.

8.3.3 AoA Estimation Accuracy and Localization Accuracy. The AoA and 2D localization accuracy are tested in the multipath-rich office space with the same modality as a comparison to the low-multipath setup in Section 8.2. In this test, one phone is attached to the user's hat with a Vive tracker to represent the best-case LOS conditions, while the other phone is in the user's pocket to simulate the real-world used case. The user moves around the
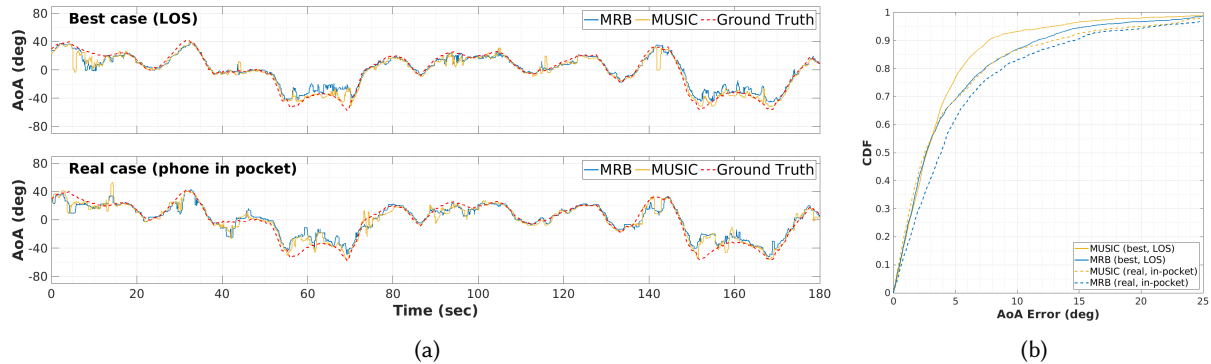
Fig. 17. 1-D AoA results in multipath-rich office space. (a) The top shows the AoA traces for the best case where the phone is in LOS condition and the bottom shows the AoA traces when the phone is in the user's pocket. The blue and yellow lines are the output of the system, and the ground truth is in red.(b) The CDF of AoA estimation error for moving targets in multipath-rich environment.

office space freely for 3 minutes. The LOS of the phone in the pocket was obstructed by desks and monitors, and the signal was attenuated by the user at all times, resulting in a challenging RF environment for the system to resolve.

Table 4 summarizes the AoA and 2D localization accuracies in the multipath-rich office space. The overall AoA accuracy drop by one degree compared to the low-multipath lobby environment in Section 8.2. The AoA traces for the best-case LOS condition and the in-pocket real-world scenario are shown in Figure 17a. Although the AoA traces follow the ground truth consistently, more noise is introduced by the environment and is particularly more challenging for the in-pocket case. The average errors of the LOS best case are 4.68° and 3.93° for MRB and modified MUSIC, and for the in-pocket case are 5.87° and 4.89° respectively. While the MRB and the modified MUSIC's average and median errors are close, the gap between the CDF of the two approaches is more significant compared to the low-multipath environment, as shown in Figure 17b. The result demonstrates the negative impact of the multipath-rich environment on AoA estimation accuracy and highlights the superiority of the modified MUSIC algorithm in resisting multipath interference.

The advantage of the modified MUSIC algorithm is further highlighted in 2D localization. Figure 18a shows the 15-second traces of both AoA approaches under the LOS best case, and Figure 18b shows the traces with the in-pocket case. The modified MUSIC approach has higher accuracy than the MRB approach, as shown in Table 4. The performance gap is further illustrated in the CDF plot shown in Figure 18c.

8.3.4 Performance with Multi-User. Tracking multiple users introduces a series of challenges to the system. In this test, five users each wore a hat attached to Vive tracker 3.0 and carried the phone in their pocket, as shown in Figure 15. The users are free to move around the space and engage in conversations with other users while other untracked personals enter and leave the space randomly. In addition to the LOS blocking from the user's body and the effect of a multipath-rich environment, the LOS blocking from other users is introduced in this experiment to test the system's ultimate performance. The average errors of AoA are 7.3° for MRB and 5.9° for modified MUSIC. The 2D localization accuracies are 83.13 cm and 68.4 cm for MRB and modified MUSIC. Overall, the system can achieve below 10 degrees AoA and sub-meter level localization accuracy with multiple users in a multipath-rich environment with commodity BLE transmitters without any modification to the device.
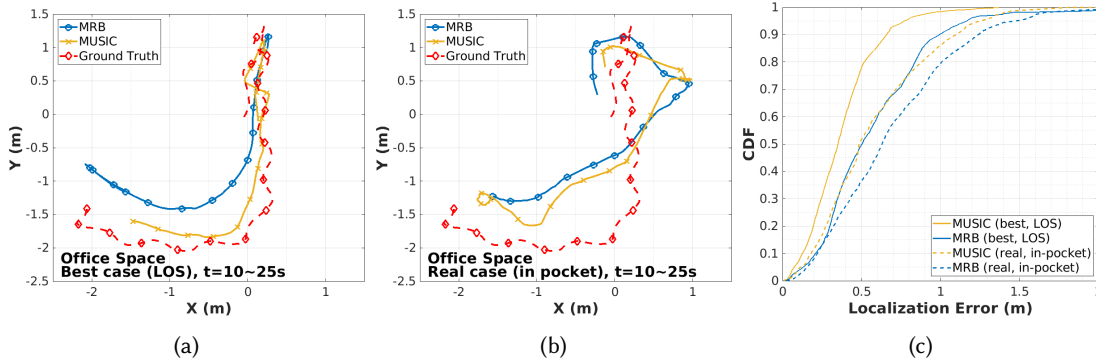
Fig. 18. 2D localization results in multipath-rich environment. (a) 2D traces for LOS condition. (b) The 2D traces of the user with the phone in the pocket. (c) The CDF of 2D localization error in the multipath-rich environment.

Table 4. AoA and Localization Accuracies for multipath-rich office space

Scenario		MRB		MUSIC	
		1D	2D	1D	2D
Best case	Average	4.68°	57.4 cm	3.93°	37.4 cm
(Phone overhead)	Median	2.64°	50.3 cm	2.70°	34.9 cm
Real case	Average	5.87°	69.4 cm	4.89°	57.7cm
(Phone in pocket)	Median	3.86°	63.0 cm	2.52°	48.5 cm

9 LIMITATIONS AND FUTURE WORK

The single packet, single channel, switched antenna array localization approach presented in this work provides several unique advantages compared to related work in terms of localization accuracy vs. receiver complexity. This can be seen in Table 1, where antenna arrays with dedicated (and synchronized) radio receivers for each antenna [31, 47] outperform our approach in terms of raw accuracy. It is reasonable to consider the performances of these fully synchronous and 1-antenna to 1-radio-receiver as an upper bound on switched antenna performance as these systems will gather more RF information and thus be able to reject multi-path interference more robustly.

In contrast, our approach outperforms fully synchronous, 1-antenna to 1-radio-receiver arrays in terms of cost and complexity. For example, Monfared et al. [31] uses 2x Ettus Research USRP X310 high-performance, software defined radios (SDRs) base, each with 2x TwinRX USRP Daughterboards, resulting in a retail price of $37,634 USD. While, our approach used an 8:1 RF Switch, and Teensy 4.1 microcontroller, and an Analog Devices PlutoSDR for a retail price of $282 USD.

One of the key advantages of our approach is that we can perform sub-packet switching to scan the entire antenna array through a single radio packet, thus allowing our system to make an Angle of Arrival estimation on a single packet, similar to fully-synchronous and 1-antenna-to-1-radio-receiver arrays. This allows our system to track and locate real-world, commercially available smartphones and IoT devices that transmit at 30 packets per second (or less) while being used in typical usage scenarios. However, the subpacket switching does introduce continuity spikes in the received waveform that requires aggressive filtering and single processing to decode correctly, and extra care must be used to decode these packets.

In an effort to create a practical, real-world indoor RF localization system, this work explores a variety of smartphone usage scenarios and environments. In the literature, it is typical to report AoA and localization numbers using sparse RF environments (free space / constrained) with low amounts of multi-path reflections

or with idealized radios, transmitting at a high power level, high packet rates and/or physically separated from the users for better RF performance. While these measures provide important performance metrics, they do not capture the expected degradation in performance caused when a users place their smartphone in their pocket or holds it in their hand while web surfing or gaming (causing shielding and attenuation of the RF waves). Our results show that while these challenging real-world usage cases do reduce accuracy in terms of raw performance, they also demonstrate sufficient AoA and localization accuracy to enable many innovative and useful indoor localization and tracking applications.

The underlining approach of sub-packet, single receiver, switched antenna arrays offer the potential for system improvements along a number of vectors. For instance, increasing the number of antennas (and thus increasing AoA accuracy) now primarily becomes a software problem rather than a hardware problem, where the goal is to increase the switch in speed so that more antennas can be cycled through a packet. For example, by doubling or tripling the switch in frequency, it should be possible to create a 16 or 24 element phased antenna array. This would also imply increasing the radio receiver bandwidth to ensure sufficient samples are collected for each antenna.

The low-cost nature of this approach while allows for system-level improvements where multiple antenna arrays (beyond the two used in this work) can be used to triangulate users with greater accuracy. As can be seen in Table 1, ArrayTrack [47] uses six antenna arrays to locate users with high accuracy. Similar results should be possible using our method but at a lower cost.

It is anticipated that the current signal processing pipeline will be applicable to other single-carrier modulations, including but not limited to OOK, ASK, BPSK, OQPSK, and DBPSK, which are commonly employed by various wireless communication standards, such as UHF RFID, Zigbee, Sigfox, and Z-wave. However, multi-carrier modulations, such as OFDM and CSS for WiFi and LoRa, can introduce phase offsets caused by sampling frequency offset (SFO) and packet boundary detection (PBD). Developing new algorithms and modifying the system structure to accommodate various RF protocols are visible paths of future work.

10 CONCLUSION

Accurate location-based services are a cornerstone technology of many innovative applications in the consumer electronics, IoT, entertainment, and healthcare domains. While researchers have shown that phased antenna arrays excel at locating mobile transmitters, the lack of cost-effective hardware that can scale to a large number of antenna elements (>4) limits the deployment and the ultimate utility of these important applications. This work argues that one of the critical bottlenecks limiting phased antennas is the requirement for synchronization between receiver signal chains or, in the case of switched antenna arrays, the need for synchronization between the RF switch and the radio receiver chain.

To address this challenge, this paper proposes an asynchronous solution where the RF switch is completely decoupled from the radio receiver at the hardware level. The key insight is that phase discontinuities are passed on to the receiver channel when the switch transitions from one antenna to another. This required sub packet switching and order to reveal all the antenna discontinuities and correct for the Carrier Frequency Offset (CFO). Finally, in order to determine the phase difference of arrival of incoming packets, a completely synthetic (aka ideal) reference packet is generated and used to create the full antenna correlation matrix for localization algorithms such as Multi-Resolution Beaming and MUSIC. Results show that the system is highly accurate, matching state-of-the-art AoA and 2D localization accuracy for phased antenna arrays with similar number of antennas. Ultimately this approach enables a single low-cost, low bandwidth commodity RF receiver to be used to create an N-element phased array for single-carrier frequency RF protocols.

ACKNOWLEDGMENTS

REFERENCES

[1] 2020. PulseLarsen W3229 patch antenna datasheet. https://www.mouser.com/datasheet/2/447/W3229-2904189.pdf.

[2] Fadel Adib, Chen-Yu Hsu, Hongzi Mao, Dina Katabi, and Frédo Durand. 2015. Capturing the Human Figure through a Wall. *ACM Trans. Graph.* 34, 6, Article 219 (oct 2015), 13 pages. https://doi.org/10.1145/2816795.2818072

[3] Alberto Alvarez-Alvarez, Jose M. Alonso, and Gracian Trivino. 2013. Human activity recognition in indoor environments by means of fusing information extracted from intensity of WiFi signal and accelerations. *Information Sciences* 233 (2013), 162 – 182. https://doi.org/10.1016/j.ins.2013.01.029

[4] Zhenlin An, Qiongzheng Lin, Ping Li, and Lei Yang. 2020. General-Purpose Deep Tracking Platform across Protocols for the Internet of Things. In *Proceedings of the 18th International Conference on Mobile Systems, Applications, and Services* (Toronto, Ontario, Canada) *(MobiSys '20)*. Association for Computing Machinery, New York, NY, USA, 94–106. https://doi.org/10.1145/3386901.3389029

[5] Akshay Athalye, Vladimir Savić, Miodrag Bolić, and Petar M Djurić. 2011. A radio frequency identification system for accurate indoor localization. In *2011 IEEE International Conference on Acoustics, Speech and Signal Processing (ICASSP)*. IEEE, 1777–1780.

[6] P. Barsocchi, S. Chessa, F. Furfari, and F. Potortì. 2013. Evaluating Ambient Assisted Living Solutions: The Localization Competition. *IEEE Pervasive Computing* 12, 4 (2013), 72–79.

[7] Chaimaa BASRI and Ahmed El Khadimi. 2016. Survey on indoor localization system and recent advances of WIFI fingerprinting technique. In *2016 5th International Conference on Multimedia Computing and Systems (ICMCS)*. 253–259. https://doi.org/10.1109/ICMCS.2016.7905633

[8] Fabio Belloni, Ville Ranki, Antti Kainulainen, and Andreas Richter. 2009. Angle-based indoor positioning system for open indoor environments. In *2009 6th Workshop on Positioning, Navigation and Communication*. IEEE, 261–265.

[9] Valentina Bianchi, Paolo Ciampolini, and Ilaria De Munari. 2018. RSSI-based indoor localization and identification for ZigBee wireless sensor networks in smart homes. *IEEE Transactions on Instrumentation and Measurement* 68, 2 (2018), 566–575.

[10] Luca Calderoni, Matteo Ferrara, Annalisa Franco, and Dario Maio. 2015. Indoor localization in a hospital environment using Random Forest classifiers. *Expert Systems with Applications* 42, 1 (2015), 125 – 134. https://doi.org/10.1016/j.eswa.2014.07.042

[11] Dongyao Chen, Kang G. Shin, Yurong Jiang, and Kyu-Han Kim. 2017. Locating and Tracking BLE Beacons with Smartphones. In *Proceedings of the 13th International Conference on Emerging Networking EXperiments and Technologies* (Incheon, Republic of Korea) *(CoNEXT '17)*. Association for Computing Machinery, New York, NY, USA, 263–275. https://doi.org/10.1145/3143361.3143385

[12] Yin Chen, Dimitrios Lymberopoulos, Jie Liu, and Bodhi Priyantha. 2012. FM-based indoor localization. In *Proceedings of the 10th international conference on Mobile systems, applications, and services*. 169–182.

[13] Krishna Chintalapudi, Anand Padmanabha Iyer, and Venkata N. Padmanabhan. 2010. Indoor Localization without the Pain. In *Proceedings of the Sixteenth Annual International Conference on Mobile Computing and Networking* (Chicago, Illinois, USA) *(MobiCom '10)*. Association for Computing Machinery, New York, NY, USA, 173–184. https://doi.org/10.1145/1859995.1860016

[14] Jeongsik Choi, Yang-Seok Choi, and Shilpa Talwar. 2019. Unsupervised Learning Technique to Obtain the Coordinates of Wi-Fi Access Points. *2019 International Conference on Indoor Positioning and Indoor Navigation (IPIN)* (2019), 1–6.

[15] Marco Cominelli, Paul Patras, and Francesco Gringoli. 2019. Dead on Arrival: An Empirical Study of The Bluetooth 5.1 Positioning System. In *Proceedings of the 13th International Workshop on Wireless Network Testbeds, Experimental Evaluation amp; Characterization* (Los Cabos, Mexico) *(WiNTECH '19)*. Association for Computing Machinery, New York, NY, USA, 13–20. https://doi.org/10.1145/3349623.3355475

[16] Buti Al Delail, Luis Weruaga, M. Jamal Zemerly, and Jason W. P. Ng. 2013. Indoor localization and navigation using smartphones augmented reality and inertial tracking. In *2013 IEEE 20th International Conference on Electronics, Circuits, and Systems (ICECS)*. 929–932. https://doi.org/10.1109/ICECS.2013.6815564

[17] N. Fallah, I. Apostolopoulos, K. Bekris, and E. Folmer. 2013. Indoor Human Navigation Systems: A Survey. *Interacting with Computers* 25, 1 (2013), 21–33.

[18] Gunter Fischer, Burkhart Dietrich, and Frank Winkler. 2004. Bluetooth indoor localization system. In *Proceedings of the 1st Workshop on Positioning, Navigation and Communication*. University of California, Berkeley, CA, US, 147–156.

[19] D. Fortin-Simard, K. Bouchard, S. Gaboury, B. Bouchard, and A. Bouzouane. 2012. Accurate passive RFID localization system for smart homes. In *2012 IEEE 3rd NESEA*.

[20] Enrique García, Pablo Poudereux, Álvaro Hernández, Jesús Ureña, and David Gualda. 2015. A robust UWB indoor positioning system for highly complex environments. In *2015 IEEE International Conference on Industrial Technology (ICIT)*. 3386–3391. https://doi.org/10.1109/ICIT.2015.7125601

[21] Jon Gjengset, Jie Xiong, Graeme McPhillips, and Kyle Jamieson. 2014. Phaser: Enabling Phased Array Signal Processing on Commodity WiFi Access Points. In *Proceedings of the 20th Annual International Conference on Mobile Computing and Networking* (Maui, Hawaii, USA) *(MobiCom '14)*. Association for Computing Machinery, New York, NY, USA, 153–164. https://doi.org/10.1145/2639108.2639139

[22] Zhihao Gu, Taiwei He, Junwei Yin, Yuedong Xu, and Jun Wu. 2021. TyrLoc: a low-cost multi-technology MIMO localization system with a single RF chain. In *Proceedings of the 19th Annual International Conference on Mobile Systems, Applications, and Services*. 228–240.

[23] Daniel Halperin, Wenjun Hu, Anmol Sheth, and David Wetherall. 2011. Tool Release: Gathering 802.11n Traces with Channel State Information. *ACM SIGCOMM CCR* 41, 1 (Jan. 2011), 53.

[24] Steven J. Henderson and Steven Feiner. 2009. Evaluating the benefits of augmented reality for task localization in maintenance of an armored personnel carrier turret. In *2009 8th IEEE International Symposium on Mixed and Augmented Reality*. 135–144. https://doi.org/10.1109/ISMAR.2009.5336486

[25] Kazuhiro Honda, Daishi Iwamoto, and Koichi Ogawa. 2017. Angle of arrival estimation embedded in a circular phased array 4 × 4 MIMO antenna. In *2017 IEEE Asia Pacific Microwave Conference (APMC)*. 93–96. https://doi.org/10.1109/APMC.2017.8251385

[26] Kang Eun Jeon, James She, Perm Soonsawad, and Pai Chet Ng. 2018. BLE Beacons for Internet of Things Applications: Survey, Challenges, and Opportunities. *IEEE Internet of Things Journal* 5, 2 (2018), 811–828. https://doi.org/10.1109/JIOT.2017.2788449

[27] Manikanta Kotaru, Kiran Joshi, Dinesh Bharadia, and Sachin Katti. 2015. SpotFi: Decimeter Level Localization Using WiFi. In *Proceedings of the 2015 ACM Conference on Special Interest Group on Data Communication* (London, United Kingdom) *(SIGCOMM '15)*. Association for Computing Machinery, New York, NY, USA, 269–282. https://doi.org/10.1145/2785956.2787487

[28] Ka-Ho Lam, Chi-Chung Cheung, and Wah-Ching Lee. 2019. RSSI-Based LoRa Localization Systems for Large-Scale Indoor and Outdoor Environments. *IEEE Transactions on Vehicular Technology* 68, 12 (2019), 11778–11791. https://doi.org/10.1109/TVT.2019.2940272

[29] X. Lin, T. Ho, C. Fang, Z. Yen, B. Yang, and F. Lai. 2015. A mobile indoor positioning system based on iBeacon technology. In *2015 37th EMBC*. 4970–4973.

[30] Ahmed Makki, Abubakr Siddig, Mohamed Saad, Joseph R Cavallaro, and Chris J Bleakley. 2015. Indoor localization using 802.11 time differences of arrival. *IEEE Transactions on Instrumentation and Measurement* 65, 3 (2015), 614–623.

[31] Shaghayegh Monfared, Trung-Hien Nguyen, Luca Petrillo, Philippe De Doncker, and François Horlin. 2018. Experimental demonstration of BLE transmitter positioning based on AOA estimation. In *2018 IEEE 29th Annual International Symposium on Personal, Indoor and Mobile Radio Communications (PIMRC)*. IEEE, 856–859.

[32] Yiran Peng, Wentao Fan, Xin Dong, and Xing Zhang. 2016. An iterative weighted KNN (IW-KNN) based indoor localization method in bluetooth low energy (BLE) environment. In *2016 Intl IEEE Conferences on Ubiquitous Intelligence & Computing, Advanced and Trusted Computing, Scalable Computing and Communications, Cloud and Big Data Computing, Internet of People, and Smart World Congress (UIC/ATC/ScalCom/CBDCom/IoP/SmartWorld)*. IEEE, 794–800.

[33] Kanyanee Phutcharoen, Monchai Chamchoy, and Pichaya Supanakoon. 2020. Accuracy Study of Indoor Positioning with Bluetooth Low Energy Beacons. In *2020 Joint International Conference on Digital Arts, Media and Technology with ECTI Northern Section Conference on Electrical, Electronics, Computer and Telecommunications Engineering (ECTI DAMT & NCON)*. IEEE, 24–27.

[34] Xinyou Qiu, Bowen Wang, Jian Wang, and Yuan Shen. 2020. AOA-based BLE localization with carrier frequency offset mitigation. In *2020 IEEE International Conference on Communications Workshops (ICC Workshops)*. IEEE, 1–5.

[35] U. Rehman and S. Cao. 2017. Augmented-Reality-Based Indoor Navigation: A Comparative Analysis of Handheld Devices Versus Google Glass. *IEEE Transactions on Human-Machine Systems* 47, 1 (2017), 140–151.

[36] T. H. Riehle, P. Lichter, and N. A. Giudice. 2008. An indoor navigation system to support the visually impaired. In *2008 30th EMBS*. 4435–4438.

[37] Lorenz Schmid, David Salido-Monzú, and Andreas Wieser. 2019. Accuracy Assessment and Learned Error Mitigation of UWB ToF Ranging. In *2019 International Conference on Indoor Positioning and Indoor Navigation (IPIN)*. 1–8. https://doi.org/10.1109/IPIN.2019.8911769

[38] Ralph Schmidt. 1986. Multiple emitter location and signal parameter estimation. *IEEE transactions on antennas and propagation* 34, 3 (1986), 276–280.

[39] Weiguang Shi, Jiangxia Du, Xiaowei Cao, Yang Yu, Yu Cao, Shuxia Yan, and Chunya Ni. 2019. IKULDAS: An Improved k NN-Based UHF RFID Indoor Localization Algorithm for Directional Radiation Scenario. *Sensors* 19, 4 (2019), 968.

[40] Petros Spachos and Konstantinos N. Plataniotis. 2020. BLE Beacons for Indoor Positioning at an Interactive IoT-Based Smart Museum. *IEEE Systems Journal* 14, 3 (2020), 3483–3493. https://doi.org/10.1109/JSYST.2020.2969088

[41] Jue Wang, Deepak Vasisht, and Dina Katabi. 2014. RF-IDraw: Virtual touch screen in the air using RF signals. *ACM SIGCOMM Computer Communication Review* 44, 4 (2014), 235–246.

[42] Xuyu Wang, Lingjun Gao, Shiwen Mao, and Santosh Pandey. 2017. CSI-Based Fingerprinting for Indoor Localization: A Deep Learning Approach. *IEEE Transactions on Vehicular Technology* 66, 1 (2017), 763–776. https://doi.org/10.1109/TVT.2016.2545523

[43] Xuyu Wang, Shiwen Mao, Santosh Pandey, and Prathima Agrawal. 2014. CA2T: Cooperative antenna arrays technique for pinpoint indoor localization. *Procedia Computer Science* 34 (2014), 392–399.

[44] Jiang Xiao, Zimu Zhou, Youwen Yi, and Lionel M. Ni. 2016. A Survey on Wireless Indoor Localization from the Device Perspective. *ACM Comput. Surv.* 49, 2, Article 25 (June 2016), 31 pages. https://doi.org/10.1145/2933232

[45] Yaxiong Xie, Zhenjiang Li, and Mo Li. 2015. Precise Power Delay Profiling with Commodity WiFi. In *Proceedings of the 21st Annual International Conference on Mobile Computing and Networking* (Paris, France) *(MobiCom '15)*. ACM, New York, NY, USA, 53–64. https://doi.org/10.1145/2789168.2790124

[46] Jie Xiong and Kyle Jamieson. 2013. {ArrayTrack}: A {Fine-Grained} Indoor Location System. In *10th USENIX Symposium on Networked Systems Design and Implementation (NSDI 13)*. 71–84.

[47] Jie Xiong and Kyle Jamieson. 2013. ArrayTrack: A Fine-Grained Indoor Location System. In *Proceedings of the 10th USENIX Conference on Networked Systems Design and Implementation* (Lombard, IL) *(nsdi'13)*. USENIX Association, USA, 71–84.

[48] Jansen Christian Liando Yaxiong Xie, Yanbo Zhang and Mo Li. 2018. SWAN: Stitched Wi-Fi ANtennas.. In *Proceedings of the 24st Annual International Conference on Mobile Computing and Networking (MobiCom '18)*. ACM.

[49] F. Zafari, A. Gkelias, and K. K. Leung. 2019. A Survey of Indoor Localization Systems and Technologies. *IEEE Communications Surveys Tutorials* 21, 3 (2019), 2568–2599.

[50] Cemin Zhang, Michael Kuhn, Brandon Merkl, Aly E Fathy, and Mohamed Mahfouz. 2006. Accurate UWB indoor localization system utilizing time difference of arrival approach. In *2006 IEEE radio and wireless symposium*. IEEE, 515–518.